JOURNAL OF COLLOID AND INTERFACE SCIENCE 155, 420–437 (1993)

Energetical and Force Approaches to the Capillary Interactions between Particles Attached to a Liquid–Fluid Interface

P. A. KRALCHEVSKY, V. N. PAUNOV, N. D. DENKOV, I. B. IVANOV,[1] AND K. NAGAYAMA*

*Laboratory of Thermodynamics and Physico-chemical Hydrodynamics, University of Sofia, Faculty of Chemistry, Sofia 1126, Bulgaria; and *Protein Array Project, ERATO, JRDC, 18-1 Higashiarai, Tsukuba 305, Japan*

Received January 10, 1992; accepted June 5, 1992

Theoretical expressions are derived for calculating the capillary meniscus interactions between two vertical cylinders or two spheres partially immersed in a liquid layer. In general, the radii and the contact angles of the two particles can be different. Two alternative approaches are followed. The first one consists in calculation of capillary interaction energy, which is then differentiated to get the force. In the second approach the force is determined directly by integrating the pressure and the interfacial tension. A very good coincidence between the numerical results of these two independent approaches is established. The results can contribute to a better understanding of phenomena like surface aggregation, surface coagulation, and formation of two-dimensional arrays at interfaces. © 1993 Academic Press, Inc.

1. INTRODUCTION

It is known from experiment that capillary interactions exist between particles attached to a fluid–liquid interface. These interactions, which usually lead to two-dimensional particle aggregation or coagulation, can be important for many processes of technological importance (1, 2). In spite of that, capillary forces have not been studied very well theoretically. This could be attributed, at least in part, to the complicated form of the Laplace equation, which governs the shape of the capillary menisci and represents a second-order nonlinear partial differential equation. Indeed, all available theoretical studies on capillary forces (3–6) deal with menisci of rotational or translational symmetry, when the Laplace equation reduces to an ordinary differential equation.

Some interesting experimental results for aggregation and ordering of colloidal particles (7–9) and protein molecules (10–12) at an interface suggest theoretical studies on the capillary interactions of particle configurations which have not yet been investigated. The present paper can be considered as a continuation of a previous study (13), where theoretical expressions for the energy of capillary interaction of two similar vertical cylinders or two similar spheres on a substrate are derived. The meniscus shape was determined by solving the Laplace partial differential equation in bipolar coordinates by using the method of matched asymptotic expansions.

Our main purpose in the present article is to generalize the results of Ref. (13) for the case when both the radii and the contact angles of the two particles are different. In Section 2 we derive asymptotic expressions describing the shape of the capillary meniscus and of the two contact lines. Then the results are applied for calculating the capillary forces by using two alternative approaches.

The first one is the *energetic approach,* based on a calculation of the total capillary (interfacial plus gravitational) energy of the system, ΔW. Then ΔW is differentiated with respect to the interparticle distance to get the capillary force. The second is the *force approach* in which the capillary force is calculated directly by integrating the force distributions: the hydrostatic pressure through the particle surface and the interfacial tension along the three-phase contact line.

Sections 3, 4, and 5 below are devoted to the derivation of expressions for ΔW in the framework of the energetic approach for the following three cases: (i) two vertical cylinders, (ii) two spheres partially immersed in a liquid layer on a substrate, and (iii) a cylinder and a sphere. The force approach is considered in Section 6, where integral expressions are derived for the forces exerted on each of the two particles. The numerical results provided by the energetic and the force approaches are compared and discussed by the end of the paper. We mention in advance that the capillary forces due to the hydrostatic pressure exerted on two particles of different sizes and/or different contact angles turn out to be of different magnitude. However, it turns out that the horizontal projections of the total capillary forces (integrals of hydrostatic pressure plus interfacial tension) have equal magnitude and opposite directions; i.e., they obey a counterpart of Newton's third law—this is proved in Appendix I.

The capillary interaction between a particle and a vertical wall is examined in a separate paper (14).

We hope the theoretical study of the capillary meniscus

[1] To whom correspondence should be addressed.

0021-9797/93 $5.00

forces will contribute to quantitative interpretation of some available experimental data and will suggest new experiments.

2. CAPILLARY MENISCUS SHAPE

(a) Basic Equations

Let us consider the capillary meniscus around two vertical circular cylinders of radii r_1 and r_2—Fig. 1. The interface is supposed to be flat and horizontal far from the cylinders. We choose the coordinate plane xy to coincide with this horizontal surface. In addition, the plane xz passes through the axes of the two cylinders. We denote by

$$z = \zeta(x, y) \qquad [2.1]$$

the equation describing the surface of the meniscus. ζ can be both positive and negative depending on the values of the contact angles α_1 and α_2—see Fig. 1.

The geometry of the system suggests the introduction of bicylindrical coordinates (τ, σ, z)—see, e.g., Refs. (13, 15):

$$x = \sqrt{g_{\tau\tau}} \sinh \tau, \quad -\infty < \tau < +\infty,$$
$$y = \sqrt{g_{\sigma\sigma}} \sin \sigma, \quad -\pi \leqslant \sigma \leqslant \pi, \qquad [2.2]$$

where

$$g_{\sigma\sigma} = g_{\tau\tau} = \frac{a^2}{(\cosh \tau - \cos \sigma)^2} \qquad [2.3]$$

and a is a constant which is determined below.

Let $\tau = -\tau_1$ and $\tau = \tau_2$ correspond to the surfaces of the left- and right-hand-side cylinders depicted in Fig. 1. Then

$$s_k = a \coth \tau_k, \quad k = 1, 2, \qquad [2.4]$$

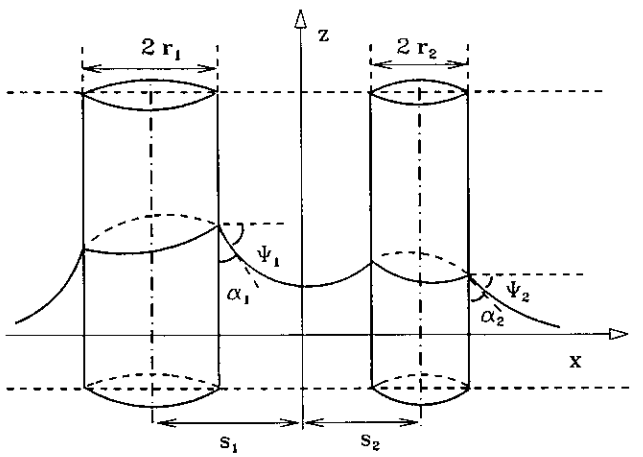

FIG. 1. Sketch of the capillary meniscus around two vertical cylinders of radii r_1 and r_2; α_1 and α_2 are three-phase contact angles.

is the distance between the z-axis and the axis of the respective cylinder—see (13, 15). Also,

$$r_k = a/\sinh \tau_k, \quad k = 1, 2. \qquad [2.5]$$

From Eqs. [2.4], [2.5] one easily derives

$$a^2 = s_1^2 - r_1^2 = s_2^2 - r_2^2. \qquad [2.6]$$

Let us denote by b the shortest distance between the two cylindrical surfaces. Then

$$s_1 + s_2 = r_1 + r_2 + b. \qquad [2.7]$$

On the other hand, from Eq. [2.6] one obtains

$$s_2^2 - s_1^2 = r_2^2 - r_1^2. \qquad [2.8]$$

By combining Eqs. [2.7] and [2.8] one derives

$$s_k = \tfrac{1}{2}[b^2 + 2(b + r_k)(r_1 + r_2)]/(b + r_1 + r_2), \quad k = 1, 2. \qquad [2.9]$$

A substitution from Eq. [2.9] into Eq. [2.6] leads to the sought-for expression determining the parameter a:

$$a^2 = \frac{b}{4}(b + 2r_1)(b + 2r_2)(b + 2r_1 + 2r_2) \Big/ (b + r_1 + r_2)^2. \qquad [2.10]$$

Having once determined a, one can calculate τ_1 and τ_2 from Eq. [2.5] and then s_1 and s_2 from Eq. [2.4].

By analogy with our previous study, Ref. (13), we investigate the case when the slope of the meniscus surface is small:

$$\left(\frac{\partial \zeta}{\partial x}\right)^2 \ll 1, \quad \left(\frac{\partial \zeta}{\partial y}\right)^2 \ll 1. \qquad [2.11]$$

In this case the Laplace equation describing the meniscus shape can be linearized,

$$\frac{\partial^2 \zeta}{\partial x^2} + \frac{\partial^2 \zeta}{\partial y^2} = q^2 \zeta \qquad [2.12]$$

—cf. Eqs. [2.5] and [2.13] in Ref. (13). Here

$$q^2 = \Delta\rho g/\gamma, \quad \Delta\rho = \rho_I - \rho_{II}, \qquad [2.13]$$

where ρ_I and ρ_{II} are the mass densities of the two neighboring fluid phases, γ is the respective interfacial tension, and g is the gravity acceleration. In bicylindrical coordinates Eq. [2.12] takes the form

$$(\cosh\tau - \cos\sigma)^2\left(\frac{\partial^2\zeta}{\partial\sigma^2} + \frac{\partial^2\zeta}{\partial\tau^2}\right) = (qa)^2\zeta(\sigma, \tau). \quad [2.14]$$

For small particles at not too large interparticle separations $(qa)^2 \ll 1$ and hence Eq. [2.14] contains a small parameter. Following the mathematical approach in Ref. (13) we consider an inner and an outer region:

inner region (close to the cylinders):

$$(\cosh\tau - \cos\sigma)^2 \gg (qa)^2$$

outer region (far from the cylinders):

$$(\cosh\tau - \cos\sigma)^2 \leqslant (qa)^2.$$

Then the method of the matched inner and outer asymptotic expansions (see, e.g., Ref. (16)) can be applied.

(b) Inner Asymptotic Solution

In the inner region Eq. [2.14] reduces to

$$\frac{\partial^2\zeta}{\partial\sigma^2} + \frac{\partial^2\zeta}{\partial\tau^2} = 0. \quad [2.15]$$

The boundary conditions at the surfaces of the two cylinders are counterparts of Eq. [3.29] in Ref. (13):

$$\left.\frac{\partial\zeta}{\partial\tau}\right|_{\tau=-\tau_1} = -\left.\sqrt{g_{\tau\tau}}\right|_{\tau=-\tau_1}\sin\psi_1$$

$$\left.\frac{\partial\zeta}{\partial\tau}\right|_{\tau=\tau_2} = \left.\sqrt{g_{\tau\tau}}\right|_{\tau=\tau_2}\sin\psi_2. \quad [2.16]$$

Here

$$\psi_k = \pi/2 - \alpha_k, \quad k = 1, 2 \quad [2.17]$$

—cf. Fig. 1. In fact, Eq. [2.16] represents the conditions for constancy of the three-phase contact angle.

Let us consider the functions

$$\zeta_k(\sigma, \tau) = C_0^{(k)} + Q_k\left[|\tau| - 2\sum_{n=1}^{\infty}\frac{e^{-n|\tau|}}{n}\cos n\sigma\right]$$

$$+ \sum_{n=1}^{\infty} C_n^{(k)}\cosh n[\tau - (-1)^k\tau_k]\cos n\sigma, \quad k = 1, 2, \quad [2.18]$$

where

$$Q_k = r_k\sin\psi_k, \quad k = 1, 2, \quad [2.19]$$

and $C_n^{(k)}$, $k = 1, 2$, $n = 0, 1, 2, \ldots$, are constants. One can check that for $\tau \neq 0$ the functions $\zeta_k(\sigma, \tau)$, $k = 1, 2$ satisfy Eq. [2.15]. In addition, a comparison with Eqs. [3.29] and [3.30] in Ref. (13) shows that $\zeta_1(\sigma, \tau)$ and $\zeta_2(\sigma, \tau)$, satisfy the boundary conditions at $\tau = -\tau_1$ and $\tau = \tau_2$, respectively. That is why one can seek the solution in the inner region in the form

$$\zeta^{\text{in}}(\sigma, \tau) = \begin{cases}\zeta_1(\sigma, \tau) & \text{for } -\tau_1 \leqslant \tau \leqslant 0\\ \zeta_2(\sigma, \tau) & \text{for } 0 \leqslant \tau \leqslant \tau_2.\end{cases} \quad [2.20]$$

The constants $C_n^{(k)}$ are to be determined from the conditions

$$\zeta_1(\sigma, 0) = \zeta_2(\sigma, 0); \quad \left.\frac{\partial\zeta_1}{\partial\tau}\right|_{\tau=0} = \left.\frac{\partial\zeta_2}{\partial\tau}\right|_{\tau=0}. \quad [2.21]$$

By substituting from Eq. [2.18] into Eq. [2.21] one determines

$$C_0^{(1)} = C_0^{(2)} \equiv C_0 \quad [2.22]$$

$$C_n^{(k)} = \frac{2(Q_2 - Q_1)}{n}\frac{(-1)^k\sinh n\tau_j}{\sinh n(\tau_1 + \tau_2)}, \quad [2.23]$$

$$j, k = 1, 2; \quad j \neq k, \; n = 1, 2, 3, \ldots.$$

The value of the constant C_0 is to be determined by matching the inner and outer asymptotic solutions. With this end in view let us investigate the asymptotic behavior of $\zeta^{\text{in}}(\sigma, \tau)$ for large $|x|$.

From Eqs. [2.18], [2.20], [2.22], and [2.23] for $\tau > 0$ one easily obtains

$$\zeta^{\text{in}}(0, \tau) = C_0 + Q_2\tau - (Q_1 + Q_2)\sum_{n=1}^{\infty}\frac{1}{n}e^{-n\tau}$$

$$+ (Q_2 - Q_1)\sum_{n=1}^{\infty}\frac{1}{n}\left[\frac{2\sinh n\tau_1\cosh n(\tau_2 - \tau)}{\sinh n(\tau_1 + \tau_2)} - e^{-n\tau}\right]. \quad [2.24]$$

Besides, according to Eq. [3.36] in Ref. (13),

$$\tau|_{y=0} = \ln\left|\frac{x + a}{x - a}\right| = 2\left[\frac{a}{x} + O\left(\frac{a^3}{x^3}\right)\right]; \quad [2.25]$$

i.e., $\tau \to 0$ when $x \to \infty$. In the same limit

$$\sum_{n=1}^{\infty}\frac{1}{n}e^{-n\tau} = -\ln(1 - e^{-\tau}) \to -\ln\tau \quad (\tau \to 0). \quad [2.26]$$

Then one obtains

$$\zeta^{\text{in}}(0, \tau) = C_0 + (Q_2 - Q_1)A$$

$$+ (Q_1 + Q_2)\left[\ln\frac{2a}{|x|} + O\left(\frac{a}{x}\right)\right], \quad [2.27]$$

where

$$A = \sum_{n=1}^{\infty} \frac{1}{n} \frac{\sinh n(\tau_1 - \tau_2)}{\sinh n(\tau_1 + \tau_2)}. \quad [2.28]$$

One can check that Eq. [2.27] holds not only for $x \to +\infty$, but also for $x \to -\infty$. Moreover, one can prove that the asymptotics of ζ^{in} for $x = 0$ and $|y| \to \infty$ are similar; i.e., the generalized form of Eq. [2.27] reads

$$(\zeta^{in})^{out} = C_0 + (Q_2 - Q_1)A + (Q_1 + Q_2)\left[\ln \frac{2a}{r} + O\left(\frac{a}{r}\right)\right], \quad [2.29]$$

where

$$r = \sqrt{x^2 + y^2}. \quad [2.30]$$

Eq. [2.30] represents the outer asymptotics of the inner solution. For two cylinders of equal radii, $A = 0$, $Q_1 = Q_2$, and Eq. [2.29] reduces to Eq. [3.41] in Ref. (13).

(c) Outer and Compound Solution

Far away from the cylinders ($r \gg r_1, r_2$) the meniscus has axial symmetry. Then in the outer region Eq. [2.12] reduces to

$$\frac{1}{r}\frac{d}{dr}\left(r\frac{d\zeta}{dr}\right) = q^2\zeta. \quad [2.31]$$

Having in mind the outer boundary condition ($\zeta \to 0$ for $r \to \infty$) from Eq. [2.31], one obtains the solution in the outer region in the form

$$\zeta^{out}(r) = GK_0(qr), \quad [2.32]$$

where G is an integration constant and K_0 is the modified Bessel function—see, e.g., (15, 17). The constant G, as well as the constant C_0 in Eq. [2.24], is to be determined by means of the condition for matching the outer and inner solutions (see Ref. (16)):

$$(\zeta^{in})^{out} = (\zeta^{out})^{in}. \quad [2.33]$$

By expanding the right-hand side of Eq. [2.32] in series for small qr, one obtains

$$(\zeta^{out})^{in} = G[-\ln(\gamma_e qr/2) + O(q^2r^2 \ln qr)], \quad [2.34]$$

where $\gamma_e = 1.781072418 \cdots$; $\ln \gamma_e$ is the Euler–Masceroni number—see, e.g., Ref. (15). Substitution from Eqs. [2.29] and [2.34] into Eq. [2.33] leads to the following expressions for the integration constants:

$$G = Q_1 + Q_2,$$

$$C_0 = (Q_1 - Q_2)A - (Q_1 + Q_2)\ln(\gamma_e qa). \quad [2.35]$$

The compound solution, which is uniformly valid in the inner and outer regions, reads (16)

$$\zeta = \zeta^{in} + \zeta^{out} - (\zeta^{out})^{in}, \quad [2.36]$$

where in agreement with Eqs. [2.34] and [2.35] one has

$$(\zeta^{out})^{in} = -(Q_1 + Q_2)\ln(\gamma_e qr/2). \quad [2.37]$$

In addition, from Eqs. [2.32] and [2.35] one obtains

$$\zeta^{out} = (Q_1 + Q_2)K_0(qr). \quad [2.38]$$

ζ^{in} is given by Eq. [2.20], where in keeping with Eq. [2.18] and the identity

$$\tau - 2\sum_{n=1}^{\infty} \frac{1}{n} e^{-n\tau} \cos n\sigma = \ln(2\cosh\tau - 2\cos\sigma)$$

ζ_1 and ζ_2 can be represented in the form

$$\zeta_k(\sigma, \tau) = C_0 + Q_k \ln(2\cosh\tau - 2\cos\sigma) + \sum_{n=1}^{\infty} C_n^{(k)} \cosh n[\tau - (-1)^k\tau_k]\cos n\sigma, \quad k = 1, 2. \quad [2.39]$$

The coefficients Q_1, Q_2, C_0 and $C_n^{(k)}$ are given by Eqs. [2.19], [2.23], and [2.35].

It is worthwhile noting that Eqs. [2.36]–[2.39] represent a zeroth-order asymptotic solution, which describes the meniscus shape with a good accuracy when Eq. [2.11] is satisfied and $(qa)^2 \ll 1$. As shown below, such is the case of colloid-sized particles, which represents an area of great practical interest.

The shape of the meniscus surface calculated from Eqs. [2.36]–[2.39] is shown in Fig. 2 as an illustration. $\psi_2 = 5°$ for Fig. 2a, whereas $\psi_2 = -5°$ for Fig. 2b. The values of the other parameters used are the same for both Figs. 2a and 2b: $r_1 = 1$ μm, $r_2 = 2$ μm, $b = 3$ μm, and $\psi_1 = 3°$. A saddle-like shape is observed between the two cylinders in Fig. 2a, whereas there is no saddle point in Fig. 2b. As proven below, the configurations shown in Figs. 2a and 2b correspond to attractive and repulsive capillary forces, respectively.

(d) Elevation of the Contact Line

Since at $\tau = -\tau_1$ and $\tau = \tau_2$, ζ^{in} depends on σ, the two contact lines are not perfectly horizontal. As was shown in Ref. (13) the deviation from horizontality is small with small particles.

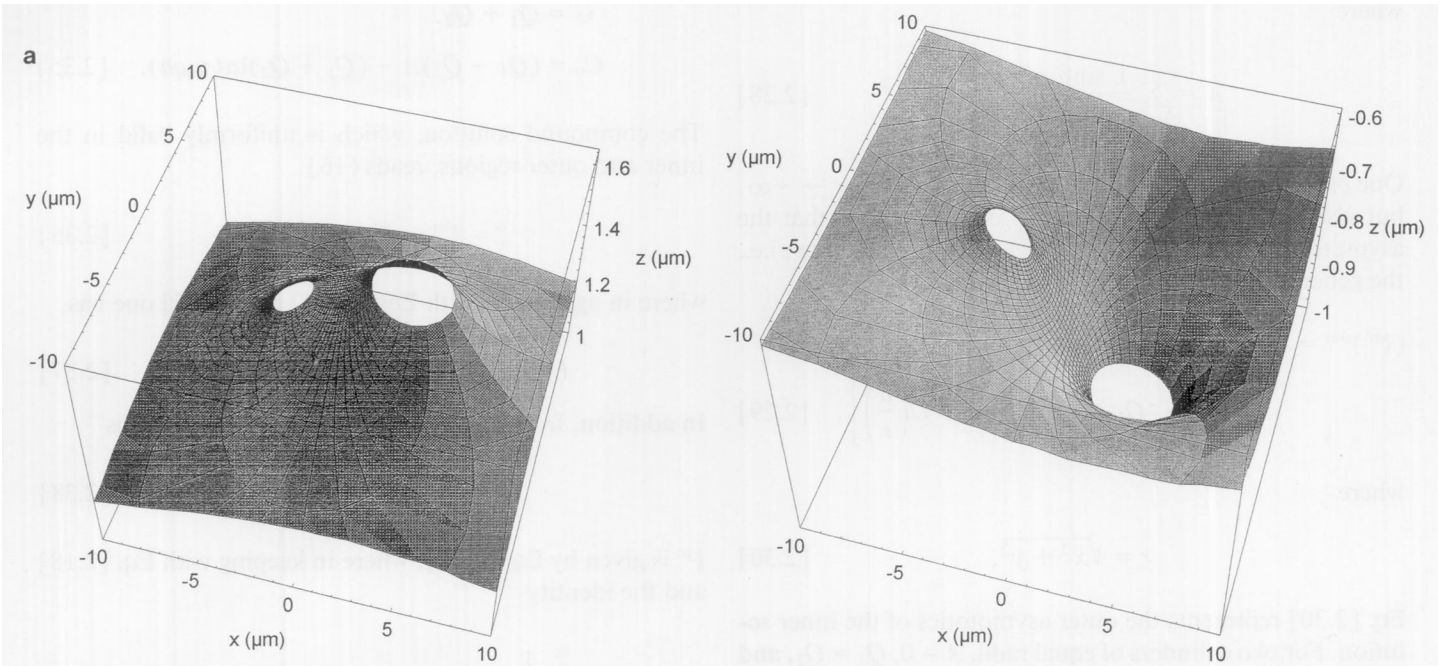

FIG. 2. The calculated shape of the capillary meniscus around two vertical cylinders. The slope angles at the contact lines are: (a) $\psi_1 = 3°$, $\psi_2 = 5°$; (b) $\psi_1 = 3°$, $\psi_2 = -5°$. In both cases $r_1 = 1$ μm, $r_2 = 2$ μm, and $b = 3$ μm.

The mean elevation of the contact lines above the horizontal surface far from the cylinders is

$$h_k = \frac{1}{2\pi r_k}\oint_{C_k} \zeta(\sigma, (-1)^k\tau_k)dl$$

$$= \frac{a}{2\pi r_k}\int_{-\pi}^{\pi} \zeta_k^{\text{in}}(\sigma, (-1)^k\tau_k)\frac{d\sigma}{\cosh\tau_k - \cos\sigma}, \quad k = 1, 2, \quad [2.40]$$

where C_k is a contour, representing the projection of the respective contact line on the coordinate plane xy. From Eqs. [2.19], [2.35], [2.39], and [2.40] one obtains

$$h_k = r_k\sin\psi_k[\tau_k + 2\ln(1 - \exp(-2\tau_k))]$$
$$- (r_1\sin\psi_1 + r_2\sin\psi_2)\ln(\gamma_e qa)$$
$$+ (r_1\sin\psi_1 - r_2\sin\psi_2)$$
$$\times\left[A - (-1)^k\sum_{n=1}^{\infty}\frac{2}{n}\frac{[\exp(-n\tau_k\sinh n\tau_j]}{\sinh n(\tau_1 + \tau_2)}\right], \quad j, k = 1, 2, \quad j \neq k, \quad [2.41]$$

where in accordance with Eq. [2.5] τ_k can be expressed as follows:

$$\tau_k = \ln\left(\frac{a}{r_k} + \sqrt{\frac{a^2}{r_k^2} + 1}\right), \quad k = 1, 2; \quad [2.42]$$

a and A are given by Eqs. [2.10] and [2.28], respectively. It is worthwhile noting that h_k can be both positive and negative—see Fig. 2b. When the two cylinders (particles) are similar ($r_1 = r_2$, $\psi_1 = \psi_2$), Eq. [2.41] reduces to Eq. [3.54] in Ref. (13).

In the limit of infinite separation between the two cylinders ($b \to \infty$) the respective limiting values $h_{k\infty}$ of h_k can be calculated by means of Derjaguin's (18) formula,

$$h_{k\infty} = r_k\sin\psi_k\ln\frac{4}{\gamma_e qr_k(1 + \cos\psi_k)}, \quad k = 1, 2, \quad (qr_k)^2 \ll 1. \quad [2.43]$$

The next term of the expansion of $h_{k\infty}$ for small $(qr_k)^2$ is derived in Refs. (19, 20). It should be noted that Eq. [2.43] cannot be derived by setting $a \to \infty$ in Eqs. [2.41] and [2.42], because Eq. [2.41] is an asymptotic formula, which is valid for $(qa)^2 \ll 1$.

As shown in Appendix II at large interparticle distances ($r_k \ll s_k \ll q^{-1}$, $k = 1, 2$), the general expression [2.41] for h_k can be expanded in series and a simple asymptotic formula is obtained:

$$h_k \approx r_k\sin\psi_k\ln(2/\gamma_e qr_k) - r_j\sin\psi_j\ln(\gamma_e qL/2), \quad [2.41a]$$

where $j, k = 1, 2; j \neq k$, and $L = b + r_1 + r_2$ is the distance between the axes of the cylinders.

In fact Eq. [2.41a] represents the elevation of the contact line at the surface of the cylinder k as a superposition of $h_{k\infty}$ (see Eq. [2.43] with $\cos\psi_k \approx 1$) and the elevation of the

meniscus at a distance L from the single cylinder j (see Appendix II).

The numerical comparison between Eq. [2.41] and its asymptotic form, Eq. [2.41a], shows that they coincide everywhere, except in the region of small separations, where the interparticle distance b is of the order of the diameter of the larger cylinder.

Figure 3 illustrates the dependence of h_1 and h_2 on the surface-to-surface separation, b, calculated from Eqs. [2.41] and [2.42]. As could be expected, h_k decreases with an increase in b. At very large b ($b \geqslant q^{-1}$), where Eq. [2.41] is no more valid, one calculates $h_k/h_{k\infty} < 1$ and even $h_k/h_{k\infty} < 0$.

The range of validity of Eq. [2.41] can be estimated in the following way. Let us choose cylinder 1 to be the one with the smaller radius ($r_1 < r_2$) and let b^* be the value of b satisfying the equation $h_1(b^*) = h_{1\infty}$, where h_k and $h_{k\infty}$ are calculated from Eqs. [2.41] and [2.43], respectively. Then for $b > b^*$ one has $h_k(b)/h_{k\infty} < 1$, which is an indication of nonapplicability of Eq. [2.41]. Hence, b^* can be used as a characteristic of the range of validity of Eq. [2.41]. Of course, b^* depends on r_1 and r_2.

Figure 4 represents b^* as a function of r_1 for different values of r_2 and for specified values of the angles ψ_1 and ψ_2. The decrease of the area below the curve $b^* = b^*(r_1)$ with increasing r_2 corresponds to a decrease of the range of validity of Eq. [2.41]. When r_1 is small, b^* is determined by the capillary length q^{-1} and does not depend on the radii r_1 and r_2.

3. CAPILLARY INTERACTION ENERGY BETWEEN TWO CYLINDERS

According to Eq. [2.4] in Ref. (13) the capillary interaction energy of a system of N particles attached to the interface between phases I and II reads

$$\Delta W = W - W_\infty, \qquad [3.1]$$

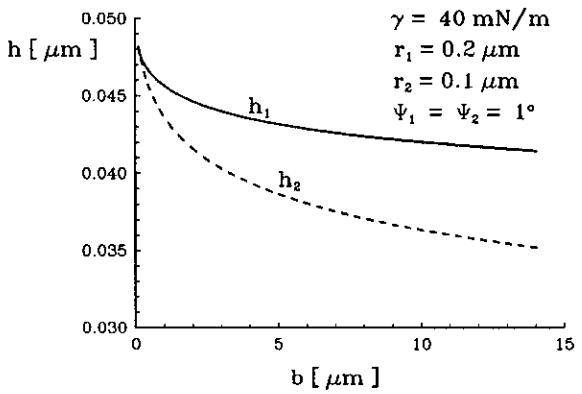

FIG. 3. Dependence of h_1 and h_2 on the surface-to-surface separation b calculated by means of Eqs. [2.41]–[2.42].

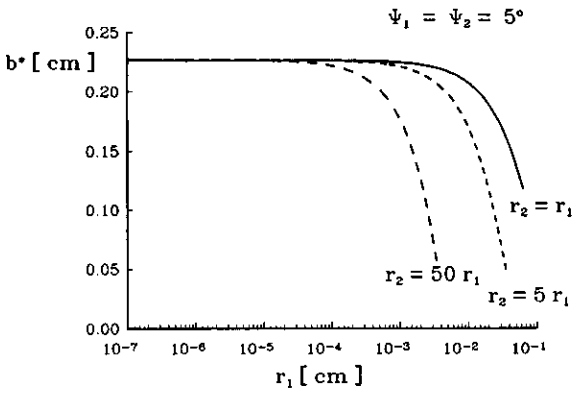

FIG. 4. Plot of b^* vs r_1 for different values of r_2; the slope angles are $\psi_1 = \psi_2 = 5°$.

with

$$W = \sum_{k=1}^{N} m_k g Z_k^{(c)} + \sum_{Y=\mathrm{I,II}} m_Y g Z_Y^{(c)} + \sum_{k=1}^{N} \sum_{Y=\mathrm{I,II}} \omega_{kY} A_{kY} + \gamma \Delta A, \qquad [3.2]$$

where W_∞ is the value of W at infinite interparticle separation; $Z_k^{(c)}$ and $Z_Y^{(c)}$, given by Eq. [2.3] in Ref. (13), are the z-coordinates of the mass centers of the respective particle or phase, whose masses are denoted by m_k and m_Y, respectively; A_{kY} and ω_{kY} are the area and the surface energy density of the interface between particle k and phase Y; γ is the interfacial tension of the boundary between phases I and II, and ΔA is the difference between the areas of the latter boundary and the portion of the plane xy included in the system. Below we calculate the contribution of each term in the right-hand side of Eq. [3.2] in the capillary interaction energy ΔW for the case of two vertical cylinders depicted in Fig. 1.

Let us start with the last term in Eq. [3.2]. This term provides a contribution

$$\Delta W_m = \gamma(\Delta A - \Delta A_\infty) \qquad [3.3]$$

to the interaction energy ΔW. (ΔA_∞ is the value of ΔA at infinite separation between cylinders.) When Eq. [2.11] is satisfied, in accordance with Eq. [2.19] of Ref. (13), one can write

$$\Delta W_m = \gamma(I - I_\infty) - \Delta\rho g\left(\int_{V_m} |z|\,dV - \int_{V_{m\infty}} |z|\,dV\right). \qquad [3.4]$$

Here $\Delta\rho$ is given by Eq. [2.13] and V_m is the volume com-

prised between the meniscus surface and its projection on the coordinate plane xy. I is an integral term, which in view of Eq. [2.18] of Ref. (13) can be represented in the form

$$I = \tfrac{1}{2} \sum_{k=1}^{2} \oint_{C_k} d\boldsymbol{l}\boldsymbol{\mu} \cdot (\zeta \nabla \zeta). \qquad [3.5]$$

Here C_k, $k = 1, 2$, are the same contours as in Eq. [2.40] above; $\boldsymbol{\mu}$ is the unit running normal to the respective contour directed inward; and ∇ is the two-dimensional gradient operator in the plane xy. If $\mathbf{e}_\tau$ is the running unit tangent to the τ-lines, then $\boldsymbol{\mu} = -\mathbf{e}_\tau$ at the contour C_1 and $\boldsymbol{\mu} = \mathbf{e}_\tau$ at the contour C_2.

By using Eq. [2.11] one derives a counterpart of Eq. [3.11] in Ref. (13):

$$\sin \psi_k = \frac{(-1)^k}{\sqrt{g_{\tau\tau}}} \frac{\partial \zeta}{\partial \tau}\bigg|_{\tau=(-1)^k \tau_k} = (-1)^k \mathbf{e}_\tau \cdot \nabla \zeta|_{\tau=(-1)^k \tau_k}. \qquad [3.6]$$

Since angles ψ_1 and ψ_2 are supposed to be constant along the respective contact lines, from Eqs. [2.40], [3.5], and [3.6] one obtains

$$I = \pi(r_1 h_1 \sin \psi_1 + r_2 h_2 \sin \psi_2). \qquad [3.7]$$

The limiting value of I for infinite separation between the two cylinders ($b \to \infty$) is

$$I_\infty = \pi(r_1 h_{1\infty} \sin \psi_1 + r_2 h_{2\infty} \sin \psi_2), \qquad [3.8]$$

where $h_{k\infty}$, $k = 1, 2$, are the respective limiting values of h_k given by Eq. [2.43].

Analogously to the derivations of Eqs. [3.19] and [3.21] in Ref. (13) one obtains

$$\sum_{k=1}^{2} \sum_{Y=\mathrm{I,II}} [\omega_{kY} A_{kY} - \lim_{b\to\infty} \omega_{kY} A_{kY}] = 2\pi \sum_{k=1}^{2} (\omega_{k\mathrm{I}} - \omega_{k\mathrm{II}})(h_k - h_{k\infty}) r_k \qquad [3.9]$$

$$\sum_{Y=\mathrm{I,II}} [m_Y g Z_Y^{(c)} - \lim_{b\to\infty} m_Y g Z_Y^{(c)}] = \Delta\rho g \left(\int_{V_\mathrm{m}} |z| dV - \int_{V_{\mathrm{m}\infty}} |z| dV \right). \qquad [3.10]$$

The first term in the right-hand side of Eq. [3.2] does not give any contribution to the capillary interaction energy ΔW, because the z-coordinates of the mass centers of the two cylinders do not depend on the distance between them. Then by combining Eqs. [3.1]–[3.4] and [3.7]–[3.10] one finally obtains

$$\Delta W = \pi \sum_{k=1}^{2} [2(\omega_{k\mathrm{I}} - \omega_{k\mathrm{II}}) + \gamma \sin \psi_k](h_k - h_{k\infty}) r_k. \qquad [3.11]$$

Note that the volume integrals in Eqs. [3.4] and [3.10] cancel each other. If the contact angles α_1 and α_2 are the equilibrium ones, i.e., if the Young equation,

$$\omega_{k\mathrm{II}} - \omega_{k\mathrm{I}} = \gamma \cos \alpha_k, \quad k = 1, 2, \qquad [3.12]$$

holds, then in view of Eq. [2.17] one can transform Eq. [3.11] to read

$$\Delta W = -\pi\gamma \sum_{k=1}^{2} (h_k - h_{k\infty}) r_k \sin \psi_k, \qquad [3.13]$$

where h_k and $h_{k\infty}$ can be calculated from Eqs. [2.41] and [2.43]. Equation [3.13] is the sought-for expression for the capillary interaction energy between two vertical cylinders as a function of the distance b between cylinder surfaces. In the case of two similar cylinders, Eq. [3.13] reduces to Eq. [3.23] in Ref. (13).

For large interparticle distances one can obtain the asymptotic expression for ΔW by substituting in Eq. [3.13] from Eq. [2.41a]. The result reads:

$$\Delta W \approx 2\pi\gamma r_1 r_2 \sin \psi_1 \sin \psi_2 \ln(\gamma_e q s), \quad r_1, r_2 \ll s \ll q^{-1}, \qquad [3.13a]$$

where $s \equiv L/2 = (s_1 + s_2)/2$—see Appendix II for more details. Equation [3.13a] shows that the capillary interaction energy is very long-range even for small particles.

Figure 5 represents the dependence of ΔW on the surface-to-surface separation, b, between two cylinders of different

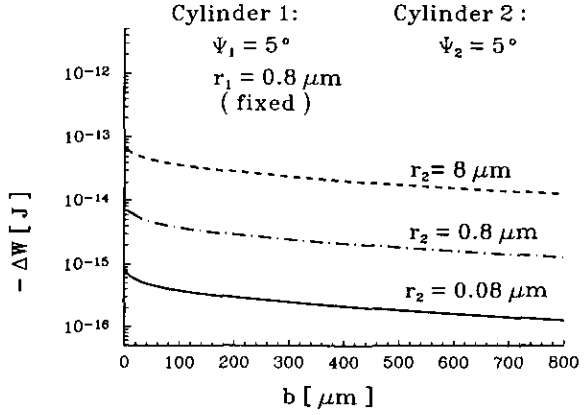

FIG. 5. Plot of the interaction energy ΔW vs the surface-to-surface separation b for different values of r_2; r_1 is fixed equal to 0.8 μm; the slope angles are $\psi_1 = \psi_2 = 5°$.

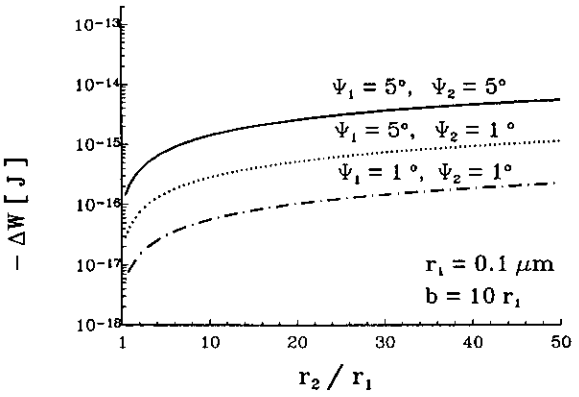

FIG. 6. Dependence of the interaction energy ΔW on r_2/r_1 at fixed radius, r_1, and for a fixed value of the surface-to-surface separation, b.

radii but equal contact angles. As could be expected, ΔW is negative (attraction) and $|\Delta W|$ decreases with increasing b. It is worth noting that the magnitude of the interaction energy is much larger than the thermal energy kT. The same is true for spherical particles (instead of cylinders—see below) and can lead to irreversible surface aggregation.

Figure 6 illustrates the behavior of ΔW when the radius of one of the cylinders is increased at a fixed radius of the other cylinder and at a fixed separation b. One sees that ΔW exhibits a tendency of leveling off for large r_2/r_1. Besides, the smaller the angles ψ_k, the smaller the capillary interaction energy $|\Delta W|$ (see also Eq. [3.13a]).

Figure 7 illustrates the dependence of ΔW on the slope angles ψ_1 and ψ_2 (respectively, on the contact angles $\alpha_k = \pi/2 - \psi_k$). One sees that ΔW is negative (attraction) when ψ_1 and ψ_2 have the same sign, ΔW is positive (repulsion) when ψ_1 and ψ_2 have opposite signs, and $\Delta W = 0$ when $\psi_1 = \psi_2 = 0$ (see also Eq. [3.13a]). The case when $\psi_1 = 0$ ($\alpha_1 = 90°$), is of special interest. In this case cylinder 1 alone does not form a meniscus; however, it still disturbs the meniscus created by cylinder 2. In fact this is the origin of the interaction between the two cylinders, which is of lower magnitude compared to the case when $\psi_1 \neq 0$—see Fig. 7.

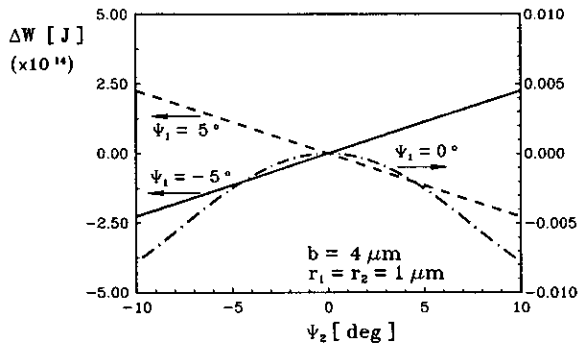

FIG. 7. Dependence of the interaction energy ΔW on the angle ψ_2 at various fixed values of the angle ψ_1; the values of the other parameters are: $b = 4\ \mu m$ and $r_1 = r_2 = 1\ \mu m$.

In the case when $\psi_1 = 0$ (and $\psi_2 \neq 0$), Eq. [3.13a] predicts $\Delta W = 0$ and does not represent the asymptotic behavior of the interaction energy. As shown in Appendix II, higher order terms in the series expansion of h_k should be taken into account. The result is

$$\Delta W \approx -\tfrac{1}{4}\pi\gamma r_1^2 r_2^2 \sin^2\psi_2 \frac{1}{s^2}; \qquad \psi_1 = 0,\ r_1, r_2 \ll s \ll q^{-1}. \quad [3.14]$$

Equation [3.14] describes very well the dashed curve (for $\psi_1 = 0$) in Fig. 7, which is calculated by using the general expression Eq. [3.13].

4. CAPILLARY INTERACTION BETWEEN PARTIALLY IMMERSED SPHERES

Let us consider a flat horizontal solid surface covered with a liquid layer of thickness l_0. In addition, let us consider two spheres of radii R_1 and R_2, which are partially immersed in the liquid layer—see Fig. 8. We investigate below the nontrivial case, when

$$l_0 < \min(2R_1, 2R_2); \quad [4.1]$$

i.e., when both particles protrude from the liquid layer and two contact lines are formed. We restrict our considerations to small particle radii,

$$(qR_k)^2 \ll 1, \quad k = 1, 2, \quad [4.2]$$

and small meniscus slopes at the contact lines,

$$\sin^2\psi_k \ll 1, \quad k = 1, 2. \quad [4.3]$$

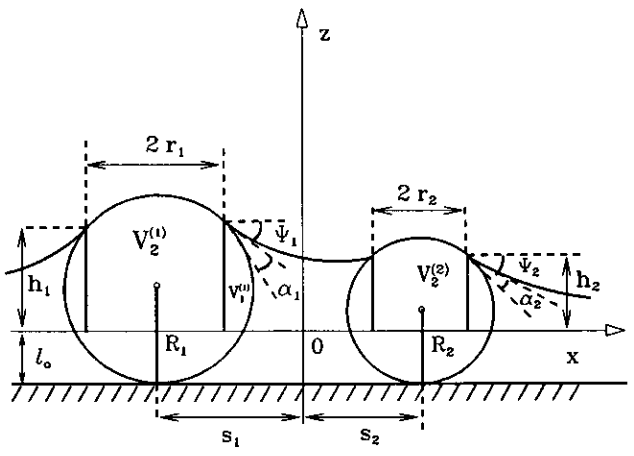

FIG. 8. Sketch of the capillary meniscus around two spherical particles partially immersed in a liquid layer on a horizontal substrate. R_k and α_k ($k = 1, 2$) are the particle radii and contact angles; l_0 is the thickness of the liquid layer far from the particles.

In this case the projections of the contact lines on the horizontal plane xy can be treated approximately as circumferences of radii r_1 and r_2 (cf. Fig. 12 in Ref. (13)). The shortest distance between the orthogonal projections of these two circumferences on the plane $z = 0$ will be denoted again by b. Instead of Eq. [2.17], in the present case one has

$$\psi_k = \arcsin\left(\frac{r_k}{R_k}\right) - \alpha_k, \quad k = 1, 2, \qquad [4.4]$$

where α_1 and α_2 are the two contact angles. We will note in advance that when the particles are small enough to satisfy Eq. [4.2], the condition for the small meniscus slope, Eq. [4.3], turns out to be satisfied automatically when $\sin^2(\alpha_2 - \alpha_1) \ll 1$, irrespective of the value of α_1.

The main difference between the case of two vertical cylinders and two spheres is that the radius of the contact line r_k and the slope angle ψ_k ($k = 1, 2$) vary with the interparticle distance. Equation [3.7] holds for both cylinders and spheres; however, instead of Eq. [3.8] in the case of spheres one is to write

$$I_\infty = \pi(r_{1\infty}h_{1\infty}\sin\psi_{1\infty} + r_{2\infty}h_{2\infty}\sin\psi_{2\infty}), \qquad [4.5]$$

where $r_{k\infty}$ and $\psi_{k\infty}$ are the limiting values of r_k and ψ_k ($k = 1, 2$) for $b \to \infty$. Then Eq. [2.19] of Ref. (13) takes the form

$$\Delta W_m = \pi\gamma \sum_{k=1}^{2} (r_k h_k \sin\psi_k - r_{k\infty}h_{k\infty}\sin\psi_{k\infty} - r_k^2 + r_{k\infty}^2) - \Delta\rho g\left(\int_{V_m} |z|\,dV - \int_{V_{m\infty}} |z|\,dV\right), \qquad [4.6]$$

where the volume integrals are the same as in Eq. [3.4] above. Equation [4.6] is a counterpart of Eq. [4.3] in Ref. (13). One can similarly derive the counterparts of Eqs. [4.4] and [4.9] in Ref. (13),

$$\sum_{k=1}^{2}\sum_{Y=I,II} (\omega_{kY}A_{kY} - \lim_{b\to\infty} \omega_{kY}A_{kY}) = 2\pi \sum_{k=1}^{2} R_k(\omega_{Ik} - \omega_{IIk})(h_k - h_{k\infty}) \qquad [4.7]$$

$$\sum_{Y=I,II} (m_Y g Z_Y^{(c)} - \lim_{b\to\infty} m_Y g Z_Y^{(c)}) = \Delta\rho g\left[\int_{V_m} |z|\,dV - \int_{V_{m\infty}} |z|\,dV + \sum_{k=1}^{2}\left(\int_{V_2^{(k)}} |z|\,dV - \int_{V_{2\infty}^{(k)}} |z|\,dV\right)\right], \qquad [4.8]$$

where $V_2^{(1)}$ and $V_2^{(2)}$ represent parts of particle volumes, which are shown in Fig. 8; $V_{2\infty}^{(k)}$ corresponds to infinite separation between the particles. Finally, in accordance with Eqs. [3.1]–[3.3] and [4.6]–[4.8] one obtains the following expression for the capillary interaction energy between the two spherical particles:

$$\Delta W = \sum_{k=1}^{2}\left[2\pi R_k(\omega_{kI} - \omega_{kII})(h_k - h_{k\infty}) - \pi\gamma(-r_k h_k \sin\psi_k + r_k^2 + r_{k\infty}h_{k\infty}\sin\psi_{k\infty} - r_{k\infty}^2) + \Delta\rho g\left(\int_{V_2^{(k)}} |z|\,dV - \int_{V_{2\infty}^{(k)}} |z|\,dV\right)\right]. \qquad [4.9]$$

When the Young equation, Eq. [3.12], is satisfied (equilibrium contact line without contact angle hysteresis), Eq. [4.9] transforms to read

$$\Delta W = -\sum_{k=1}^{2}\left\{\pi\gamma[2(h_k - h_{k\infty})R_k\cos\alpha_k - r_k h_k\sin\psi_k + r_k^2 + r_{k\infty}h_{k\infty}\sin\psi_{k\infty} - r_{k\infty}^2] - \Delta\rho g\left(\int_{V_2^{(k)}} |z|\,dV - \int_{V_{2\infty}^{(k)}} |z|\,dV\right)\right\}. \qquad [4.10]$$

The volume integral term in Eq. [4.10] (which is often negligible) can be easily calculated:

$$\int_{V_2^{(k)}} |z|\,dV - \int_{V_{2\infty}^{(k)}} |z|\,dV = \frac{\pi}{2}\left\{\frac{1}{2}(h_{k\infty}^2 - h_k^2)[2l_0(2R_k - l_0) - h_k^2 - h_{k\infty}^2] + \frac{4}{3}(R_k - l_0)(h_{k\infty}^2 - h_k^2) + r_k^2 h_k^2 - r_{k\infty}^2 h_{k\infty}^2\right\}, \quad k = 1, 2. \qquad [4.11]$$

Since the energy of capillary interaction between the two particles, ΔW, depends on the distance

$$L = r_1 + r_2 + b = s_1 + s_2 \qquad [4.12]$$

between the centers of the particles, the corresponding capillary force can be calculated by differentiation:

$$F = -\frac{d(\Delta W)}{dL}. \qquad [4.13]$$

By the end of Section 6 below it is demonstrated that the capillary force F calculated from Eq. [4.13] coincides with the force obtained by direct integration of the hydrostatic

pressure through the particle surface and of the interfacial tension along the contact line.

To determine the interaction energy ΔW one first calculates some geometric parameters. A calculative procedure is proposed below.

The input geometric parameters are the distance between the spheres, L, the thickness of the layer far from the particles, l_0, the particle radii, R_k, and the contact angles, α_k, $k = 1, 2$. The parameters $h_{k\infty}$, $r_{k\infty}$, and $\psi_{k\infty}$ are calculated by means of Eqs. [5.1]–[5.4] of Ref. (13). To determine h_k, r_k, and ψ_k we used the following procedure.

From the equation of the sphere one finds

$$r_k(h_k) = [(l_0 + h_k)(2R_k - l_0 - h_k)]^{1/2}, \quad k = 1, 2. \quad [4.14]$$

Then from Eq. [4.4] one calculates

$$\psi_k(h_k) = \arcsin \frac{r_k(h_k)}{R_k} - \alpha_k, \quad k = 1, 2. \quad [4.15]$$

For a given value of b, Eq. [2.41], along with Eqs. [2.10], [2.28], and [2.42], determines h_k as a function of r_k and ψ_k, $k = 1, 2$:

$$h_k = F_k(r_1(h_1), r_2(h_2), \psi_1(h_1), \psi_2(h_2)), \quad k = 1, 2. \quad [4.16]$$

Equations [4.14]–[4.16] represent a set of six equations for calculating the six parameters, h_k, r_k, and ψ_k, $k = 1, 2$. One can solve the problem by using numerical minimization of the function

$$\Phi(h_1, h_2) = \sum_{k=1}^{2} [h_k - F_k(r_1(h_1), r_2(h_2), \psi_1(h_1), \psi_2(h_2))]^2. \quad [4.17]$$

In view of Eq. [4.16] the minimum value of $\Phi(h_1, h_2)$ is zero; the couple (h_1^*, h_2^*) satisfying the equation $\Phi(h_1^*, h_2^*) = 0$ in fact represents the solution of Eq. [4.16]. To find (h_1^*, h_2^*) we varied h_k between $-l_0$ and $2R_k - l_0$, $k = 1, 2$, by using the method of Hooke and Jeeves (21).

5. CAPILLARY INTERACTION BETWEEN VERTICAL CYLINDER AND SPHERE

The method developed above can be directly applied to calculate the capillary interaction between a vertical cylinder and a partially immersed sphere. The system is depicted in Fig. 9. The geometrical parameters belonging to the cylinder and the sphere are denoted by indices 1 and 2, respectively. Thus r_1 and R_2 denote the radii of the cylinder and the sphere; α_k and ψ_k ($k = 1, 2$) are the respective contact and meniscus slope angles—see Fig. 9. r_2 and L have the same meaning as in the previous section; a can be calculated by means of

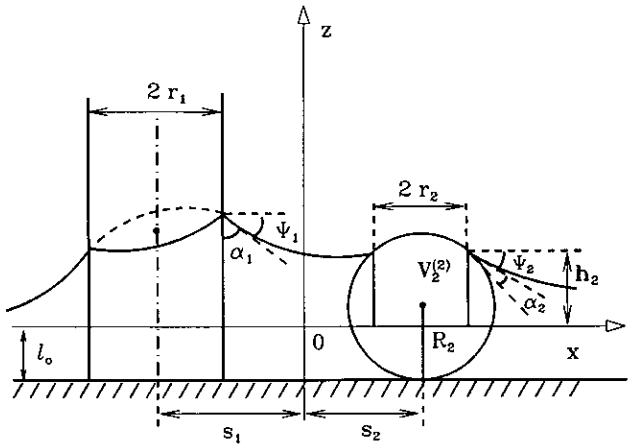

FIG. 9. Sketch of a cylinder and a sphere, which are partially immersed in a liquid layer on a horizontal substrate; l_0 is the layer thickness far from the cylinder and particle.

Eq. [2.10]. We suppose again that $(qa)^2 \ll 1$ and that Eq. [4.3] is satisfied. Then, by analogy with the derivations of Eqs. [3.14] and [4.10], one obtains the following expression for the energy of capillary interaction between the sphere and the cylinder:

$$\Delta W = -\pi\gamma[(h_1 - h_{1\infty})r_1 \sin\psi_1 - h_2 r_2 \sin\psi_2 + h_{2\infty} r_{2\infty} \sin\psi_{2\infty} + 2(h_2 - h_{2\infty})R_2 \cos\alpha_2 - r_{2\infty}^2 + r_2^2] + \Delta\rho g\left[\int_{V_2^{(2)}} |z|\,dV - \int_{V_{2\infty}^{(2)}} |z|\,dV\right]. \quad [5.1]$$

The last term in Eq. [5.1] can be calculated by means of Eq. [4.11] for $k = 2$. The parameters $r_{2\infty}$, $\psi_{2\infty}$, and $h_{2\infty}$ can be determined by means of Eqs. [5.1]–[5.4] in Ref. (13). $h_{1\infty}$ can be calculated directly from Eq. [2.43]. Since $r_1 = \text{const}$ and $\psi_1 = \text{const}$, Eqs. [4.14]–[4.15] for $k = 2$ together with Eq. [4.16], form a set of four equations determining the four parameters r_2, ψ_2, h_1, and h_2 for each given distance L. This set can be solved by means of a numerical minimization procedure based on a counterpart of Eq. [4.17].

As an illustration Fig. 10 represents the dependence of the capillary interaction energy ΔW on the distance, L, between a sphere and a vertical cylinder. One sees that ΔW is negative (attraction) and $|\Delta W|$ increases with an increase of the particle radius R_2. Also, $|\Delta W|$ is again much larger than the thermal energy kT; i.e., the capillary force prevails over the Brownian force exerted on the particle.

6. CAPILLARY FORCES

As far as we deal with distributed forces (hydrostatic pressure, interfacial tension), the derivative

$$d(\Delta W)/dL$$

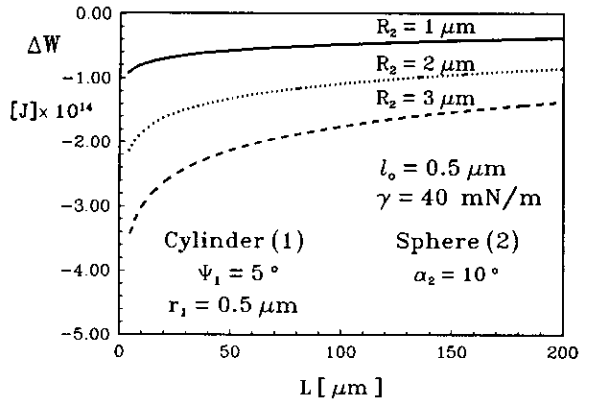

FIG. 10. Plot of the capillary interaction energy ΔW vs the distance, L, between a cylinder of radius $r_1 = 0.5$ μm and a spherical particle of radius R_2; the values of the other parameters are: $\psi_1 = 5°$, $\alpha_2 = 10°$, $l_0 = 0.5$ μm.

of the total interaction energy with respect to the interparticle distance in Eq. [4.13] in general must not be equal to the capillary force exerted on one of the two particles. Indeed, ΔW includes the capillary (surface plus gravitational) energy not only of the particles, but also of the capillary meniscus and of the two adjacent phases.

The capillary force exerted on one of the particles can be obtained by integrating the meniscus interfacial tension along the contact line and the hydrostatic pressure through the particle surface,

$$\mathbf{F}^{(k)} = \mathbf{F}^{(k\gamma)} + \mathbf{F}^{(kp)}, \quad k = 1, 2, \qquad [6.1]$$

where

$$\mathbf{F}^{(k\gamma)} = \int_{L_k} \gamma dl, \quad \mathbf{F}^{(kp)} = -\int_{S_k} d\mathbf{s}p. \qquad [6.2]$$

Here L_k and S_k ($k = 1, 2$) symbolize the respective contact line and particle surface, γ is the meniscus surface tension considered as a vector, and p is the hydrostatic pressure. It should be noted that $\mathbf{F}^{(k)}$ is a force, which is liable to direct measurement.

As discussed by the end of this section, it turns out that due to the special properties of the Laplace equation and its boundary conditions the force approach based on Eqs. [6.1] and [6.2] and the energetic approach based on Eq. [4.13] gives the same result for the capillary force—see also Appendix I.

First, we calculate $\mathbf{F}^{(k)}$ for each of the two cylinders depicted in Fig. 1. For the sake of convenience we make a special choice of the coordinate system—see Fig. 11. The z-axis coincides with the axis of the cylinder of consideration. The plane $z = 0$ as usual coincides with the horizontal fluid interface far from the cylinders. The x-axis is directed from the cylinder of consideration toward the other cylinder. Then the symmetry of the system implies that the y-components of $\mathbf{F}^{(k\gamma)}$ and $\mathbf{F}^{(kp)}$ must be equal to zero. That is why our task is reduced to the calculation of

$$F_x^{(k\gamma)} = \mathbf{e}_x \cdot \mathbf{F}^{(k\gamma)} \quad \text{and} \quad F_x^{(kp)} = \mathbf{e}_x \cdot \mathbf{F}^{(kp)}, \qquad [6.3]$$

where $\mathbf{e}_x$ is the unit vector of the x-axis. Due to the specific choice of the coordinate system, the positive (negative) value of $F_x^{(k)}$ corresponds to capillary attraction (repulsion) between the two cylinders.

(a) Force Due to Interfacial Tension

Let $z = \zeta(\varphi)$ be the equation of the contact line with φ being the azimuthal angle in the plane xy—see Fig. 11. Then the linear element along the contact line is

$$dl = \chi d\varphi, \quad \chi = \left[r_k^2 + \left(\frac{d\zeta}{d\varphi} \right)^2 \right]^{1/2}. \qquad [6.4]$$

The vector of the running unit tangent to the contact line is

$$\mathbf{t} = \frac{1}{\chi} \left(-r_k \sin\varphi \mathbf{e}_x + r_k \cos\varphi \mathbf{e}_y + \frac{d\zeta}{d\varphi} \mathbf{e}_z \right), \qquad [6.5]$$

with $\mathbf{e}_x$, $\mathbf{e}_y$, and $\mathbf{e}_z$ being the unit vectors of the respective axes. Similarly, the vector of the running unit normal to the cylindrical surface is

$$\mathbf{n} = \cos\varphi \mathbf{e}_x + \sin\varphi \mathbf{e}_y. \qquad [6.6]$$

At a given point M of the contact line one can define the vector of the unit running binormal as follows:

$$\mathbf{b} = \mathbf{t} \times \mathbf{n}. \qquad [6.7]$$

Since the vector of the interfacial tension γ belongs to the plane formed by the vectors $\mathbf{n}$ and $\mathbf{b}$, one can write

$$\gamma = \gamma(\sin\psi_k \mathbf{b} + \cos\psi_k \mathbf{n}) \qquad [6.8]$$

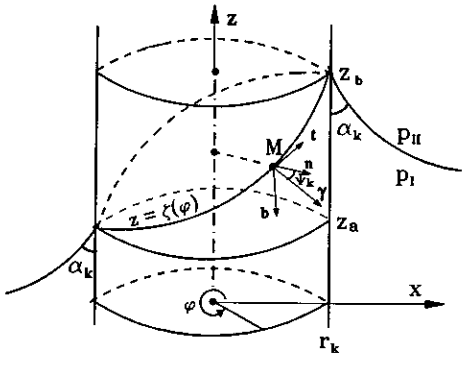

FIG. 11. Sketch of the contact line $z = \zeta(\varphi)$ on a vertical cylinder of radius r_k and contact angle α_k. The slope of the contact line is exaggerated.

—see Fig. 11. Then by substituting from Eqs. [6.5]–[6.7] into Eq. [6.8] one obtains

$$\gamma_x \equiv \mathbf{e}_x \cdot \boldsymbol{\gamma} = \gamma\left(\cos\varphi\cos\psi_k - \frac{1}{\chi}\frac{d\zeta}{d\varphi}\sin\varphi\sin\psi_k\right). \quad [6.9]$$

From Eqs. [6.2]–[6.4] and [6.9] one derives

$$F_x^{(k\gamma)} = -2\gamma\sin\psi_k\int_0^{\pi}\frac{d\zeta}{d\varphi}\sin\varphi d\varphi + \Delta F_x^{(k)},$$

where

$$\Delta F_x^{(k)} = \gamma\cos\psi_k\int_0^{2\pi}\chi\cos\varphi d\varphi \approx \gamma\frac{1}{r_k}\int_0^{\pi}\left(\frac{d\zeta}{d\varphi}\right)^2\cos\varphi d\varphi \quad [6.10]$$

—cf. Eqs. [2.11] and [4.3]. At the last step we expanded the square root in Eq. [6.4] into a series.

Above we derived the expression for calculating ζ in bipolar coordinates (σ, τ). Now it is more convenient to use σ for the parameterization of the contact line (at $\tau = (-1)^k\tau_k = \text{const}$, $k = 1, 2$), instead of the azimuthal angle φ. From Eqs. [2.2]–[2.4], one can obtain the connection between the two parameters, φ and σ:

$$\cos\varphi = \frac{1 - \cosh\tau_k\cos\sigma}{\cosh\tau_k - \cos\sigma}, \qquad 0 \leqslant \varphi \leqslant \pi, \quad \pi \geqslant \sigma \geqslant 0, \quad [6.11]$$

where τ_k is given by Eq. [2.42]. A combination of Eqs. [6.10] and [6.11] yields

$$F_x^{(k\gamma)} = 2\gamma\sin\psi_k\sinh\tau_k\int_0^{\pi}\frac{d\zeta}{d\sigma}\frac{\sin\sigma d\sigma}{\cosh\tau_k - \cos\sigma} + \Delta F_x^{(k)}, \qquad k = 1, 2. \quad [6.12]$$

In addition, from Eq. [2.39] one obtains

$$\frac{d\zeta}{d\sigma} \equiv \left.\frac{\partial\zeta_k}{\partial\sigma}\right|_{\tau=(-1)^k\tau_k} = Q_k\frac{\sin\sigma}{\cosh\tau_k - \cos\sigma} - \sum_{n=1}^{\infty} nC_n^{(k)}\sin n\sigma. \quad [6.13]$$

By substituting from Eq. [6.13] into Eq. [6.12] and by using Eq. [2.23] and the identities

$$\int_0^{\pi}\frac{\sin^2\sigma d\sigma}{(\cosh\tau - \cos\sigma)^2} = \frac{\pi e^{-\tau}}{\sinh\tau},$$

$$\int_0^{\pi}\frac{\sin n\sigma\sin\sigma d\sigma}{\cosh\tau - \cos\sigma} = \pi e^{-n\tau},$$

one derives

$$F_x^{(k\gamma)} = 2\pi\gamma\sin\psi_k\left[Q_k e^{-\tau_k} + 2(Q_1 - Q_2)(-1)^k\sinh\tau_k \times\sum_{n=1}^{\infty}\frac{e^{-2n\tau_k} - E^{(n)}}{1 - E^{(n)}}\right] + \Delta F_x^{(k)} \quad [6.14]$$

$(k = 1, 2)$; where Q_k and τ_k are given by Eqs. [2.19] and [2.42], and

$$E^{(n)} = e^{-2n(\tau_1+\tau_2)},$$

$$\Delta F_x^{(k)} = \frac{\gamma}{a}\int_0^{\pi}\left(\frac{d\zeta}{d\sigma}\right)^2(1 - \cosh\tau_k\cos\sigma)d\sigma.$$

The last integral can be calculated numerically after substituting the expression for $d\zeta/d\sigma$ from Eq. [6.13]. Equation [6.14] represents the sought-for contribution of the interfacial tension into the horizontal projection of the capillary force.

At a large interparticle separation one can obtain a simple asymptotic expression for $F_x^{(k\gamma)}$ as explained in Appendix II. The final result is

$$F_x^{(k\gamma)} \approx \pi\gamma r_1 r_2\sin\psi_1\sin\psi_2\frac{1}{s}. \quad [6.14a]$$

The latter expression for $F_x^{(k\gamma)}$ coincides with the derivative $d(\Delta W)/dL$ of the interaction energy expressed by means of Eq. [3.13a] $(L = 2s)$. This means that $F_x^{(k\gamma)}$ dominates the capillary forces, at least for large interparticle separations. Equation [6.14a] shows that $F_x^{(k\gamma)}$ decays very slowly with the inverse first power of the interparticle distance. Thus, the capillary forces turn out to have a very long-range.

(b) Force Due to Hydrostatic Pressure

Below we proceed with the derivation of an expression for $\mathbf{F}^{(kp)}$. Let z_a and z_b be the z-coordinates of the highest and of the lowest point of the contact line—see Fig. 11. S_k in Eq. [6.2] can be chosen to be part of the cylinder surface, comprised between the planes $z = z_a$ and $z = z_b$. The hydrostatic pressure in the two neighboring fluid phases is

$$p_Y = p_0 - \rho_Y g z, \quad Y = \text{I, II}, \quad [6.15]$$

where $p_0 = \text{const}$ is the pressure at the level $z = 0$. Then in Eq. [6.2] one is to substitute for p the expression

$$p = \begin{cases} p_{\text{I}} & \text{for } z_a \leqslant z \leqslant \zeta(\varphi) \\ p_{\text{II}} & \text{for } \zeta(\varphi) \leqslant z \leqslant z_b, \end{cases} \quad [6.16]$$

where as usual $z = \zeta(\varphi)$ is the equation of the contact line. Accordingly, from Eqs. [6.2]–[6.3] one obtains

$$F_x^{(kp)} = -\int_{-\pi}^{\pi} d\varphi r_k \cos\varphi \left[\int_{z_a}^{\zeta(\varphi)} p_I dz + \int_{\zeta(\varphi)}^{z_b} p_{II} dz \right]. \quad [6.17]$$

By substituting from Eq. [6.15] into Eq. [6.17] one derives

$$F_x^{(kp)} = \Delta\rho g r_k \int_0^{\pi} \zeta^2(\varphi) \cos\varphi d\varphi, \quad [6.18]$$

where $\Delta\rho$ is the same as in Eq. [2.13]. On the other hand, by differentiating Eq. [6.11] one obtains

$$\frac{d\varphi}{d\sigma} = -\frac{\sinh\tau_k}{\cosh\tau_k - \cos\sigma}. \quad [6.19]$$

Finally, Eqs. [2.5], [6.11], [6.18], and [6.19] yield

$$F_x^{(kp)} = \Delta\rho g a \int_0^{\pi} \frac{1 - \cosh\tau\cos\sigma}{(\cosh\tau - \cos\sigma)^2} \zeta_k^2 d\sigma,$$
$$\tau = (-1)^k \tau_k, \quad [6.20]$$

$k = 1, 2$; ζ_k is given by Eq. [2.39] above.

The series expansion of Eq. [6.20] for a large separation between the cylinders leads to the following asymptotic expression for $F_x^{(kp)}$ (see Appendix II):

$$F_x^{(kp)} \approx \pi\gamma(qr_k)^2 h_k r_j \sin\psi_{js}^{\frac{1}{2}}, \quad k = 1, 2; j \neq k. \quad [6.20a]$$

The comparison between Eq. [6.20a] and Eq. [6.14a] shows that the ratio

$$F_x^{(kp)}/F_x^{(k\gamma)} \approx \frac{(qr_k)^2 h_k}{r_k \sin\psi_k}$$

is usually a small quantity ($(qr_k)^2 \ll 1$) and decreases slowly with the distance between the cylinders (see also Eq. [2.41a]).

(c) Application to Spherical Particle

As explained in Sections 4 and 5 above, the expression for the meniscus profile $\zeta(\sigma, \tau)$ in the case of two vertical cylinders can be also applied for approximate calculation of the capillary interactions between two spheres on a substratum or between a sphere and a cylinder. Similarly, when the deviation of the contact line from the horizontal is not too large, one can use Eqs. [6.14] and [6.20] for approximate calculation of $F_x^{(k\gamma)}$ and $F_x^{(kp)}$ for two interacting spheres as well as for a sphere and a cylinder. In particular, the applicability of Eq. [6.20] needs additional discussion. Indeed, the horizontal projection of the force exerted on an element ds_s from the surface of a sphere is $p\cos\theta ds_s = pds_c$—see Fig. 12. Here $ds_c = (ds_s)\cos\theta$ is the area of the orthogonal projection of ds_s on the surface of the respective cylinder (z_a and z_b in Fig. 12 are the same as in Fig. 11). Hence the integration taken through the spherical belt can be approximately replaced by the integral through the surface of the cylinder comprised between the planes $z = z_a$ and $z = z_b$. In other words, Eq. [6.17] and its corollary, Eq. [6.20], can be used also in the case of a spherical particle.

(d) Discussion and Numerical Results

It should be noted that Eqs. [4.13], [6.1], and [6.2] represent two alternative approaches for calculating the capillary interactions: an energetic and a force approach. First of all, Eq. [4.13] makes sense if $F_x^{(1)} = F_x^{(2)}$; i.e., if the capillary meniscus interactions obey a counterpart of Newton's third law. It is proven in Appendix I that this condition is really satisfied, at least for a small slope of the meniscus surface. This is a nontrivial result, because it is not obvious why $F_x^{(1)}$ and $F_x^{(2)}$ are to coincide when the radii and the contact angles of the two cylinders (particles) are different. Besides, it turns out that only the sum $F_x^{(kp)} + F_x^{(k\gamma)}$ satisfies a counterpart of Newton's law, whereas $F_x^{(kp)}$ and $F_x^{(k\gamma)}$ separately do not. ($F_x^{(1p)} \neq F_x^{(2p)}$, etc.) This is illustrated below by means of some numerical results.

Figure 13a represents $F_x^{(kp)}$ for $k = 1, 2$, calculated from Eq. [6.20] for two cylinders of different radii but of equal contact angles. One sees that the hydrostatic pressure force exerted on the cylinder of larger radius is larger. Both $F_x^{(1p)}$ and $F_x^{(2p)}$ are of the order of 10^{-16} N and are much smaller than $F_x^{(k\gamma)}$ shown in Fig. 13b for the same two cylinders as calculated from Eq. [6.14]. As could be expected, $F_x^{(1\gamma)} = F_x^{(2\gamma)}$ in agreement with Newton's law (see Appendix I). More precisely there is a small difference between $F_x^{(1\gamma)}$ and $F_x^{(2\gamma)}$ which is due to the difference between $F_x^{(1p)}$ and $F_x^{(2p)}$; this difference is too small and cannot be visualized in Fig. 13b. We recall that in the notation of the present section the positive sign of $F_x^{(k\gamma)}$ corresponds to attraction between the two cylinders (particles).

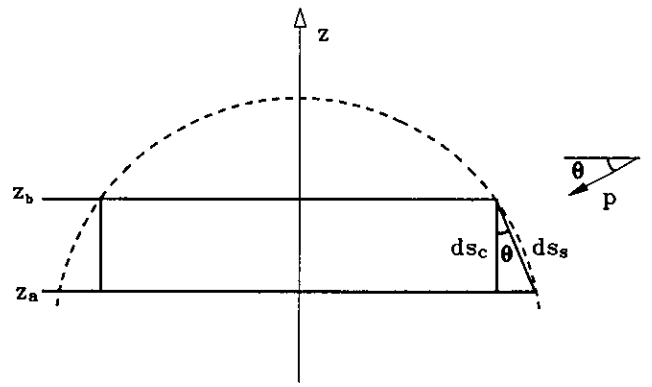

FIG. 12. Cross section of a spherical particle. The pressure p is directed normally to the spherical surface element ds_s.

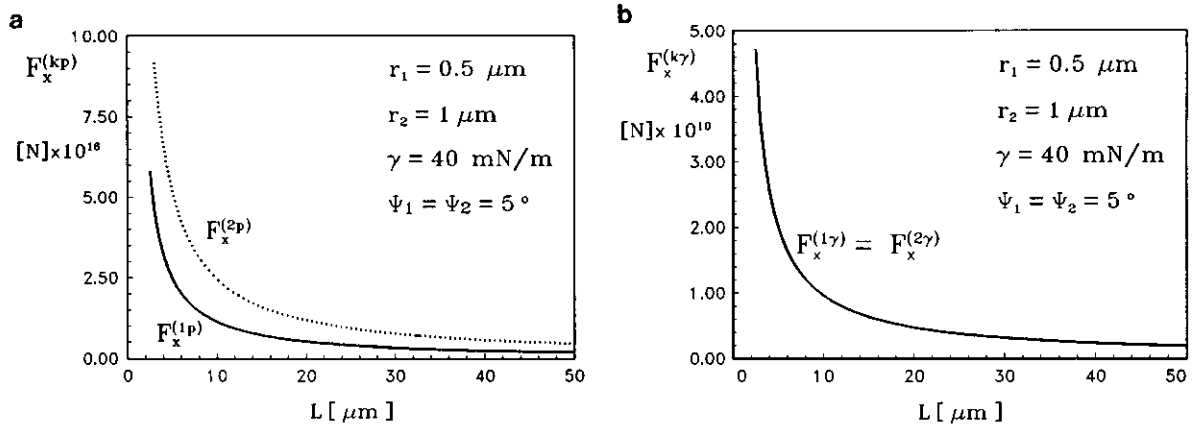

FIG. 13. Plot of capillary force vs distance L between two vertical cylinders of different radii but equal contact angles: (a) $F_x^{(kp)}$ calculated from Eq. [6.20], (b) $F_x^{(k\gamma)}$ calculated from Eq. [6.14].

Figure 14 illustrates the fact that the capillary forces can be both attractive and repulsive depending on the sign of the slope angles ψ_1 and ψ_2. As could be expected, both $F_x^{(kp)}$ and $F_x^{(k\gamma)}$ are repulsive when ψ_1 and ψ_2 are of different signs.

In addition, we calculated the capillary force by differentiating the capillary energy ΔW numerically in accordance with Eqs. [3.13] and [4.13]. The result turned out to be in very good agreement with the numerical data for $F_x^{(k)} = F_x^{(k\gamma)} + F_x^{(kp)}$. As an illustration the values of $F_x^{(1)}$, $F_x^{(2)}$, and $d(\Delta W)/dL$ are compared in Table 1 for the case of two vertical cylinders of different radii ($r_1 = 10\ \mu m$, $r_2 = 30\ \mu m$) and different contact angles ($\psi_1 = 10°$, $\psi_2 = 1°$). $F_x^{(1)}$ and $F_x^{(2)}$ are calculated by means of Eqs. [6.14] and [6.20]. The data in Table 1 confirm the equivalence of the force and energetic approaches to the calculation of the capillary interactions. In other words, one can write

$$F_x^{(1)} = F_x^{(2)} = \frac{d(\Delta W)}{dL}. \qquad [6.21]$$

The numerical coincidence between the three forces in Eq. [6.21] represents also a confirmation of the reliability of the asymptotic expressions derived in Section 2 above.

It is worth mentioning that the approximate expressions [6.14a] and [6.20a] are very accurate except in the case of small separations between the cylinders.

To calculate $F_x^{(k)}$ or ΔW one needs the values of the geometrical parameters r_k, ψ_k, and h_k. As pointed out above, the values of these parameters depend on the geometrical configuration of the system: two vertical cylinders, two spherical particles on a horizontal substrate, etc. It is worthwhile noting that a similar calculative procedure is applicable also to spherical particles floating on a liquid–fluid interface. In this case the geometrical configuration of the system can be determined from the balance between the gravity force (particle weight plus buoyancy) and the vertical component of the interfacial tension acting on the three-phase contact line:

$$2\pi r_k \gamma \sin \psi_k = F_g. \qquad [6.22]$$

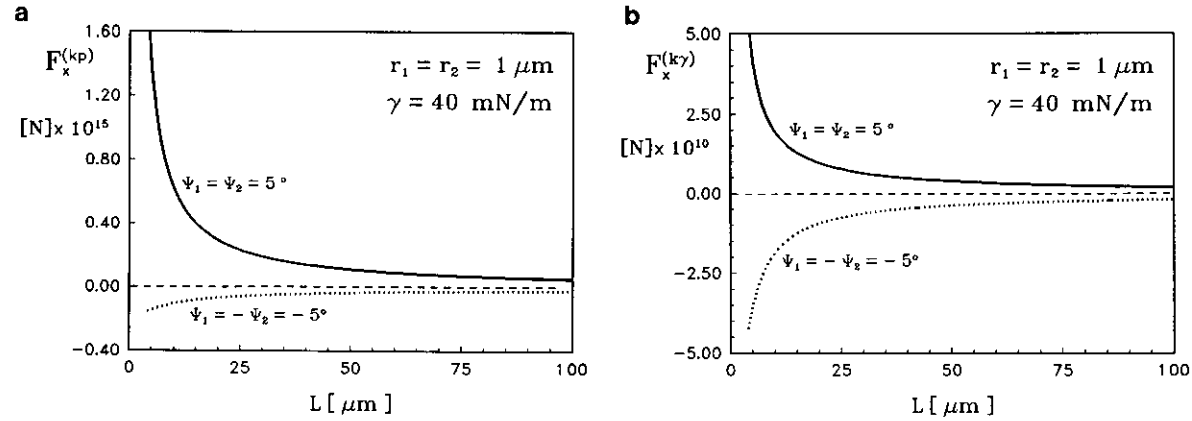

FIG. 14. Plot of capillary force vs distance L between two vertical cylinders of equal radii at various contact angles: (a) $F_x^{(kp)}$ calculated from Eq. [6.20]; (b) $F_x^{(k\gamma)}$ calculated from Eq. [6.14].

TABLE 1
Comparison between $F_x^{(1)}$, $F_x^{(2)}$, and $d\Delta W/dL$ for $r_1 = 10$ μm, $r_2 = 30$ μm, $\psi_1 = 10°$, $\psi_2 = 1°$

s (μm)	$F_x^{(1)}$ (N)	$F_x^{(2)}$ (N)	$d\Delta W/dL$ (N)
50	1.482×10^{-8}	1.485×10^{-8}	1.483×10^{-8}
100	3.054×10^{-9}	3.061×10^{-9}	3.054×10^{-9}
150	1.737×10^{-9}	1.742×10^{-9}	1.737×10^{-9}
200	1.231×10^{-9}	1.234×10^{-9}	1.231×10^{-9}
250	9.590×10^{-10}	9.612×10^{-10}	9.588×10^{-10}
300	7.876×10^{-10}	7.893×10^{-10}	7.875×10^{-10}
350	6.692×10^{-10}	6.706×10^{-10}	6.691×10^{-10}
400	5.822×10^{-10}	5.834×10^{-10}	5.821×10^{-10}
450	5.155×10^{-10}	5.165×10^{-10}	5.154×10^{-10}
500	4.626×10^{-10}	4.635×10^{-10}	4.625×10^{-10}

The following expression for F_g is available (see, e.g., Eq. [32] in Ref. (22)):

$$F_g = g[(\rho_I - \rho_p)V_l + (\rho_{II} - \rho_p)V_u - (\rho_I - \rho_{II})\pi r_k^2 h_k]. \quad [6.23]$$

Here ρ_p is the particle mass density and V_l and V_u are the parts of the particle volume situated, respectively, below and above the level of the contact line. We believe that the application of the above approach to a reexamination of the problem for capillary forces between freely floating particles deserves special attention and can be the subject of a subsequent paper.

7. CONCLUDING REMARKS

This article presents a theoretical study of the capillary meniscus interactions between two particles attached to a liquid–fluid interface. Theoretical expressions for calculating the capillary forces acting between two vertical cylinders, between a cylinder and a sphere, and between two spheres are derived. In general these expressions hold for particles of different contact angles and different radii of the contact lines. On the other hand, the validity of these expressions is limited to the case of a small slope of the meniscus surface (cf. Eq. [2.11]) and to particle radii and interparticle separations which are small compared with the capillary length q^{-1}—cf. Eq. [2.13]. For a liquid–gas interface q^{-1} is of order of 1 mm. Hence our asymptotic expressions are valid for particles with radii of the order of 100 μm or smaller. Fortunately, this range of radii corresponds to systems of considerable scientific and practical importance connected with processes of interfacial aggregation and interfacial separation of particles.

To calculate the capillary interactions between two particles one first determines the shape of the capillary meniscus. In fact this is the main theoretical problem connected with capillary forces. The forementioned restrictions for small slope and small radii enabled us to solve the problem by using bipolar coordinates in conjunction with the method of matched asymptotic expansions. The derived compound solution, given by Eqs. [2.36]–[2.39], can be applied to calculating the meniscus shape in any case, when the horizontal projection of each of the two contact lines is circular irrespective of the shape of the particles. Equations [2.36]–[2.39] allow calculation of the meniscus profile—see Fig. 2. This provides a possibility for comparison between the theory and experiment because the meniscus shape can be determined experimentally by means of different interferometric (23) or holographic (24) techniques. A combination between theory and experiment can produce a method for direct determination of the microparticle contact angle.

Having once determined the meniscus profile, one can calculate the capillary forces by using the two alternative approaches: the energetic one and the force one. In this paper we have followed the two approaches in parallel and have compared the results.

The energetic approach is based on a general expression for the total capillary energy ΔW—see Eq. [2.4] in our previous paper, Ref. (13). Here this expression is specified for three geometical configurations: (i) two vertical cylinders, Eq. [3.13]; (ii) two different spheres, Eq. [4.10]; and (iii) a cylinder and a sphere, Eq. [5.1]. It is worth noting that the capillary energy ΔW turns out to be much larger in magnitude than the thermal energy, kT, even for submicrometer particles—see Figs. 5–7 and 10.

The force approach, which is physically more transparent, provides expressions for direct calculation of the capillary forces—see Eqs. [6.1], [6.14], and [6.20]. It turns out that for micrometer-sized particles the contribution of the hydrostatic pressure to the capillary force is much smaller than the contribution of the interfacial tension—see Figs. 13 and 14. Besides, it turns out that in spite of the different radii and contact angles of the two particles, the capillary forces exerted on them are equal. In other words, they obey a counterpart of Newton's third law, at least for small slopes of the meniscus surface—the theoretical proof is given in Appendix I. This result reveals why the energetic approach makes sense. Indeed, the total capillary energy ΔW can be considered as a potential of the capillary forces—see Eq. [6.21]. The numerical test of Eq. [6.21] (see Table 1) demonstrates a very good agreement between the results of the energetical and force approaches. This is also an argument in favor of the reliability of our asymptotic expressions for the meniscus shape. For large separations between the particles, simple asymptotic expressions for the capillary interaction energy and forces are obtained by expanding in series the general equations and keeping the leading terms—see Eqs. [2.41a], [3.13a], [3.14], [6.14a], and [6.20a]. The numerical comparison of these asymptotic expressions with the respective general formulas, Eqs. [2.41], [3.13], [6.14], and [6.20], shows very good agreement except in the case of small interparticle separations. We hope the results can be generalized for the case of multiparticle capillary meniscus interactions.

APPENDIX I: THE CAPILLARY FORCES AND NEWTON'S THIRD LAW

Let $\mathbf{F}_{\mathrm{II}}^{(k)}$ ($k = 1, 2$) be the projection of the capillary force $\mathbf{F}^{(k)}$ on the horizontal coordinate plane xy. (The choice of the coordinate system is the same as in Fig. 1.) Our aim here is to prove that the horizontal projections of capillary forces exerted on the two cylinders (or spherical particles) obey a counterpart of Newton's third law; i.e., that

$$\mathbf{F}_{\mathrm{II}}^{(2)} = -\mathbf{F}_{\mathrm{II}}^{(1)}. \qquad [A.1]$$

It will be demonstrated that Eq. [A.1] holds because the shape of the capillary meniscus surface satisfies the Laplace equation along with the condition for constancy of the three-phase contact angles. We will consider again the case when the slope of the meniscus surface is small—cf. Eq. [2.11]. On the other hand, our derivation is not limited to small particle radii, r_k, or to a small interparticle distance, L.

From Eqs. [6.1]–[6.2] one obtains

$$\mathbf{F}_{\mathrm{II}}^{(k)} = \oint_{L_k} dl\boldsymbol{\gamma}_{\mathrm{II}} + \oint_{C_k} dl\boldsymbol{\mu} \int_{z_a}^{z_b} dzp, \quad k = 1, 2. \qquad [A.2]$$

Here L_k denotes the respective contact line and C_k is its orthogonal projection on the horizontal plane xy; $\boldsymbol{\mu}$, z_a, and z_b are the same as in Eqs. [3.5] and [6.17]; $\boldsymbol{\gamma}_{\mathrm{II}}$ is a vector representing the horizontal projection of the interfacial tension γ.

Let us first consider the left-hand-side cylinder (particle). From Eqs. [6.5]–[6.8] one can derive

$$\boldsymbol{\gamma}_{\mathrm{II}} = \gamma\left(\mathbf{e}_\sigma \frac{d\zeta}{dl} \sin\psi_1 + \mathbf{e}_\tau \cos\psi_1\right), \quad \tau = -\tau_1, \qquad [A.3]$$

where $\mathbf{e}_\sigma$ and $\mathbf{e}_\tau$ are the running unit vectors tangential to the σ and τ lines in bipolar coordinates—cf. Eq. [2.2]. In our case $\mathbf{e}_\sigma$ and $\mathbf{e}_\tau$ represent also the units tangent and normal to the contour C_1. In particular,

$$\oint_{C_1} dl\mathbf{e}_\tau = 0, \qquad [A.4]$$

$$\frac{d\zeta}{dl} = \frac{1}{\lambda}\frac{\partial\zeta}{\partial\sigma}, \quad \lambda = \sqrt{g_{\tau\tau}}, \quad \tau = -\tau_1 \qquad [A.5]$$

—cf. also Eq. [2.3]. In addition,

$$\oint_{L_1} dl\boldsymbol{\gamma}_{\mathrm{II}} = \oint_{C_1} \frac{dl}{\cos\theta}\boldsymbol{\gamma}_{\mathrm{II}} = \oint_{C_1} dl\boldsymbol{\gamma}_{\mathrm{II}}\left[1 + \left(\frac{d\zeta}{dl}\right)^2\right]^{1/2}, \qquad [A.6]$$

where the angle θ characterizes the running slope of the contact line L_1. By expanding the square root in Eq. [A.6] and by using Eqs. [A.3] and [A.4] one obtains

$$\oint_{L_1} dl\boldsymbol{\gamma}_{\mathrm{II}} = \gamma \oint_{C_1} dl\left[\mathbf{e}_\sigma \frac{d\zeta}{dl}\sin\psi_1 + \mathbf{e}_\tau \frac{1}{2}\left(\frac{d\zeta}{dl}\right)^2\right], \qquad [A.7]$$

where the higher order terms with respect to the slope are neglected—cf. Eq. [2.11]. Then having in mind the constancy of angle ψ_1 from Eqs. [3.6], [A.5], and [A.7], one derives

$$\oint_{L_1} dl\boldsymbol{\gamma}_{\mathrm{II}} = \gamma \oint_{C_1} dl\left\{\left(\mathbf{e}_\sigma \frac{1}{\lambda}\frac{\partial\zeta}{\partial\sigma} + \mathbf{e}_\tau \frac{1}{\lambda}\frac{\partial\zeta}{\partial\tau}\right)\sin\psi_1 + \mathbf{e}_\tau \frac{1}{2\lambda^2}\left[\left(\frac{\partial\zeta}{\partial\sigma}\right)^2 + \left(\frac{\partial\zeta}{\partial\tau}\right)^2\right]\right\}.$$

The last equation can be transformed to read

$$\oint_{L_1} dl\boldsymbol{\gamma}_{\mathrm{II}} = \gamma \oint_{C_1} dl[-\mathbf{e}_\tau\cdot(\nabla\zeta)\nabla\zeta + \tfrac{1}{2}\mathbf{e}_\tau(\nabla\zeta)\cdot\nabla\zeta], \qquad [A.8]$$

where ∇ is the gradient operator in the plane xy and Eq. [3.6] was used again. On the other hand, similarly to Eq. [6.18], one can derive

$$\oint_{C_1} dl\boldsymbol{\mu} \int_{z_a}^{z_b} dzp = -\Delta\rho g \oint_{C_1} dl\boldsymbol{\mu}\tfrac{1}{2}\zeta^2. \qquad [A.9]$$

Equations [2.13], [A.2], and [A.8]–[A.9] yield

$$\mathbf{F}_{\mathrm{II}}^{(1)} = \gamma \oint_{C_1} dl\boldsymbol{\mu} \cdot \{(\nabla\zeta)\nabla\zeta - \tfrac{1}{2}\mathbf{U}[(\nabla\zeta)\cdot\nabla\zeta + q^2\zeta^2]\}, \qquad [A.10]$$

where $\boldsymbol{\mu} = -\mathbf{e}_\tau$ and $\mathbf{U}$ is the idemfactor (the unit tensor) in the plane xy. Analogous considerations lead to an expression for $\mathbf{F}_{\mathrm{II}}^{(2)}$, which can be obtained by formally changing the index 1 to 2 in Eq. [A.10]. Then

$$\mathbf{F}_{\mathrm{II}}^{(1)} + \mathbf{F}_{\mathrm{II}}^{(2)} = \gamma \sum_{k=1}^{2} \oint_{C_k} dl\boldsymbol{\mu} \cdot \{(\nabla\zeta)\nabla\zeta - \tfrac{1}{2}\mathbf{U}[(\nabla\zeta)\cdot\nabla\zeta + q^2\zeta^2]\}. \qquad [A.11]$$

As is known, ζ tends exponentially to zero far from the cylinders—see, e.g., Eq. [2.38]. Then by using Green's theorem (see, e.g., Ref. (25)) one can transform Eq. [A.11] to read

$$\mathbf{F}_{\mathrm{II}}^{(1)} + \mathbf{F}_{\mathrm{II}}^{(2)} = -\gamma \int_{S_\infty} ds\{\nabla\cdot[(\nabla\zeta)\nabla\zeta] - \tfrac{1}{2}\nabla[(\nabla\zeta)\cdot\nabla\zeta + q^2\zeta^2]\}, \qquad [A.12]$$

where S_m is the orthogonal projection of the meniscus surface on the plane xy. From the Laplace equation, Eq. [2.12], it follows

$$\nabla \cdot [(\nabla\zeta)\nabla\zeta] = q^2\zeta\nabla\zeta + (\nabla\zeta)\cdot\nabla\nabla\zeta. \qquad [A.13]$$

Besides,

$$\nabla[(\nabla\zeta)\cdot\nabla\zeta] = 2(\nabla\zeta)\cdot\nabla\nabla\zeta. \qquad [A.14]$$

Then Eq. [A.13] takes the form

$$\nabla \cdot [(\nabla\zeta)\nabla\zeta] = \tfrac{1}{2}\nabla[q^2\zeta^2 + (\nabla\zeta)\cdot(\nabla\zeta)]. \qquad [A.15]$$

The substitution from Eq. [A.15] into Eq. [A.12] leads to the sought-for relation, Eq. [A.1], representing Newton's law.

APPENDIX II: CAPILLARY INTERACTIONS AT LARGE INTERPARTICLE SEPARATION

When two cylinders, like those shown in Fig. 1, are separated at a large distance from one another, i.e., when

$$\epsilon_k \equiv \frac{r_k}{s_k} \ll 1, \quad k = 1, 2, \qquad [B.1]$$

simple asymptotic formulas for the capillary energy and force can be obtained by using appropriate series expansions.

Equation [2.6] can be transformed to read

$$a^2 = s_1^2(1 - \epsilon_1^2) = s_2^2(1 - \epsilon_2^2). \qquad [B.2]$$

Let us consider the simplest case when $\epsilon_1 \sim \epsilon_2 \ll 1$. From Eq. [B.2] one obtains

$$a \approx s_k[1 + O(\epsilon_k^2)]. \qquad [B.3]$$

One sees from Eq. [B3] that at large interparticle distances

$$a \approx s_1 \approx s_2 \approx \frac{L}{2} \equiv s, \qquad [B.4]$$

where L is the distance between the axes of the cylinders—cf. Eq. [4.12] and Fig. 1. Then from Eq. [2.42] one derives

$$\tau_k \approx \ln\left\{\frac{2}{\epsilon_k}[1 + O(\epsilon_k^2)]\right\} \qquad [B.5]$$

$$\sinh \tau_k \approx \cosh \tau_k \approx \frac{1}{\epsilon_k}[1 + O(\epsilon_k^2)]. \qquad [B.6]$$

By substituting from Eqs. [B.4]–[B.6] into Eqs. [2.23], [2.28], and [2.35] one can derive expressions for the constants A, C_0, and $C_n^{(k)}$:

$$A \approx \tfrac{1}{4}\{\epsilon_2^2 - \epsilon_1^2\} + O(\epsilon_k^4) \qquad [B.7]$$

$$C_0 \approx -(Q_1 + Q_2)\ln\{\gamma_e qs[1 + O(\epsilon_k^2)]\} + O(Q_k\epsilon_k^2) \qquad [B.8]$$

$$C_n^{(k)} \approx (-1)^k \frac{2}{n}(Q_2 - Q_1)\left(\frac{\epsilon_k}{2}\right)^n [1 + O(\epsilon_k^2)], \qquad [B.9]$$

where Q_k are defined by Eq. [2.19].

Equations [B.4]–[B.9] can be used to obtain the asymptotics of the general expressions for the capillary interaction energy and forces derived in the paper. Thus, Eq. [2.41] expressing the mean elevation of the three-phase contact lines can be simplified to read

$$h_k \approx r_k \sin\psi_k \ln(2/\gamma_e q r_k) - r_j \sin\psi_j \ln(\gamma_e qs) + O(Q_k\epsilon_k^2), \quad k = 1, 2; j \neq k. \qquad [B.10]$$

Equation [B.10] can be written in the form

$$h_k \approx h_{k\infty} + \Delta h_j(L), \qquad [B.11]$$

where $h_{k\infty}$ is the elevation of the contact line at a single cylinder k (compare the first term in the right-hand side of Eq. [B.10] with Eq. [2.43] for $\cos\psi_k \approx 1$) and $\Delta h_j(L) = r_j \sin\psi_j K_0(qL)$ is the elevation of the meniscus surface at a distance L from a single cylinder j (see, e.g., Ref. (20)). In fact, the second term in the right-hand side of Eq. [B.10] contains the leading term in the expansion of the modified Bessel function $K_0(x)$ for small values of $x = qL$. Equation [B.11] means that at large distances between the particles, the superposition approximation for the shape of the meniscus holds.

To get an asymptotic expression for the shape of the contact line at the cylinder surfaces we are to set $\tau = -\tau_1$ or $\tau = \tau_2$ in Eq. [2.39] and to expand in series. Thus by using Eqs. [2.19] and [B.4]–[B.10] one obtains

$$\zeta_k^c = \zeta_k(\sigma, \tau = (-1)^k\tau_k) \approx h_k - r_k r_j \sin\psi_j \frac{\cos\sigma}{s}. \qquad [B.12]$$

It can be easily shown that for similar cylinders the inclination of the contact line, characterized by means of the angle η_k is small compared with the slope of the meniscus at the cylinder surface. η_k is defined through the relation:

$$\tan\eta_k = [\zeta_k^c(\pi) - \zeta_k^c(0)]/2r_k. \qquad [B.13]$$

By using Eqs. [B.12] and [B.13] one obtains

$$\frac{\tan\eta_k}{\sin\psi_k} \approx \frac{\eta_k}{\psi_k} \approx \frac{r_k}{s} = \epsilon_k \qquad [B.14]$$

—cf. Eq. [B.1]. The asymptotic form of the interaction en-

ergy between the two cylinders can be obtained by combining Eq. [3.13] with Eq. [B.10] (see also Eq. [2.43]). The result reads:

$$\Delta W \approx 2\pi\gamma r_1 r_2 \sin\psi_1 \sin\psi_2 \ln(\gamma_e q s) + O(Q_k^2 \epsilon_k^2). \quad [B.15]$$

By differentiating Eq. [B.15], along with Eq. [B.4], one obtains an approximate formula for the capillary force acting between the cylinders:

$$F = \frac{d\Delta W}{dL} \approx \pi\gamma r_1 r_2 \sin\psi_1 \sin\psi_2 \frac{1}{s}[1 + O(\epsilon_k^2)]. \quad [B.16]$$

The same result (Eq. [B.16]) can be obtained by expansion in series of Eq. [6.14] for $F_x^{(k\gamma)}$. Since $(qr_k)^2 \ll 1$ the other component of the capillary force, $F_x^{(kp)}$ (see Eq. 6.20]),

$$F_x^{(kp)} \approx \pi\gamma (qr_k)^2 h_k r_j \sin\psi_j \frac{1}{s}[1 + O(\epsilon_k)], \qquad k = 1, 2; j \neq k, \quad [B.17]$$

is much smaller than $F_x^{(k\gamma)}$ (i.e., $F_x^{(k\gamma)} \approx F$)—cf. Eqs. [B.16]—[B.17].

If $\psi_j \ll \psi_k$ and/or $r_j \ll r_k$, the higher order terms in the expansions should be also taken into account. For example, it stems from Eq. [3.13] that the energy of capillary interaction between two vertical cylinders is given by the expression

$$\Delta W \approx 2\pi\gamma Q_1 Q_2 \ln(\gamma_e q s) - \tfrac{1}{4}\pi\gamma\{Q_1^2\epsilon_2^2 + Q_2\epsilon_1^2\} + O(Q_k^2\epsilon_k^4). \quad [B.18]$$

Let ψ_1 (and Q_1) be equal to zero. Then Eq. [B.18] takes the form

$$\Delta W \approx -\tfrac{1}{4}\pi\gamma r_1^2 r_2^2 \sin^2\psi_2 \frac{1}{s^2} + O(Q_2^2\epsilon_k^4); \quad \psi_1 = 0. \quad [B.19]$$

The differentiation of Eq. [B.19] with respect to the interparticle distance L yields the capillary force, in this case:

$$F \approx \tfrac{1}{4}\pi\gamma r_1^2 r_2^2 \sin^2\psi_2 \frac{1}{s^3}; \quad \psi_1 = 0. \quad [B.20]$$

The numerical calculations show that the asymptotic expressions, Eqs. [B.10]–[B.20], although quite simple, describe very well the capillary interactions except at very small interparticle distances. It should also be kept in mind that the asymptotic formulas, as well as the general expressions, are restricted to small slopes of the meniscus profile ($\sin^2\psi_k \ll 1$, $k = 1, 2$) and to not very large interparticle distances ($qL \ll 1$); i.e., the approximate expressions [B.3]–[B.20] are strictly applicable for interparticle distances L in the region

$$r_k \ll L \ll q^{-1}. \quad [B.21]$$

ACKNOWLEDGMENT

This work was supported by the Research and Development corporation of Japan (JRDC) under the Nagayama Protein Array Project as part of the program "Exploratory Research for Advanced Technology" (ERATO).

REFERENCES

1. Gerson, D. F., Zaijc, J. E., and Ouchi, M. D., *in* "Chemistry for Energy" (M. Tomlinson, Ed.), ACS Symposium Series, Vol. 90, p. 77. Am. Chem. Soc., Washington, DC, 1979.
2. Henry, J. D., Prudich, M. E., and Vaidyanathan, K. P., *Sep. Purif. Methods* **8,** 81 (1979).
3. Nicolson, M. M., *Proc. Cambridge Philos. Soc.* **45,** 288 (1949).
4. Gifford, W. A., and Scriven, L. E., *Chem. Eng. Sci.* **26,** 287 (1971).
5. Chan, D. Y. C., Henry, J. D., and White, L. R., *J. Colloid Interface Sci.* **79,** 410 (1981).
6. Fortes, M. A., *Can. J. Chem.* **60,** 2889 (1982).
7. Pieranski, P., *Phys. Rev. Lett.* **45,** 569 (1980).
8. Onoda, G. Y., *Phys. Rev. Lett.* **55,** 226 (1985).
9. Hayashi, S., Kumamoto, Y., Suzuki, T., and Hirai, T., *J. Colloid Interface Sci.* **144,** 538 (1991).
10. Yoshimura, H., Endo, S., Matsumoto, M., Nagayama, K., and Kagawa, Y., *J. Biochem.* **106,** 958 (1989).
11. Yoshimura, H., Matsumoto, M., Endo, S., and Nagayama, K., *Ultramicroscopy* **32,** 265 (1990).
12. Haggerty, L., Watson, B. H., Barteau, M. A., and Lenhoff, A. M., *J. Vac. Sci. Technol.* **B9,** 1219 (1991).
13. Kralchevsky, P. A., Paunov, V. N., Ivanov, I. B., and Nagayama, K., *J. Colloid Interface Sci.* **151,** 79 (1992).
14. Paunov, V. N., Kralchevsky, P. A., Denkov, N. D., Ivanov, I. B., and Nagayama, K., *Colloids Surf.*, in press.
15. Korn, G. A., and Korn, T. M., "Mathematical Handbook." McGraw-Hill, New York, 1968.
16. Nayfeh, A. H., "Perturbation Methods." Wiley, New York, 1973.
17. Abramovitz, M., and Stegun, I. A., "Handbook of Mathematical Functions." Dover, New York, 1965.
18. Derjaguin, B., *Dokl. Akad. Nauk USSR* **51,** 517 (1946).
19. Lo, L. L., *J. Fluid Mech.* **132,** 65 (1983).
20. Kralchevsky, P. A., Ivanov, I. B., and Nikolov, A. D., *J. Colloid Interface Sci.* **112,** 108 (1986).
21. Hooke, R., and Jeeves, T. A., *J. Assoc. Comp. Mach.* **8,** 212 (1961).
22. Ivanov, I. B., Kralchevsky, P. A., and Nikolov, A. D., *J. Colloid Interface Sci.* **112,** 97 (1986).
23. Divitrov, A. S., Kralchevsky, P. A., Nikolov, A. D., and Wasan, D. T., *Colloids Surf.* **47,** 299 (1990).
24. Hinsch, K., *J. Colloid Interface Sci.* **92,** 243 (1983).
25. McConnell, A. J., "Application of Tensor Analysis." Dover, New York, 1957.